

# Reinforcement learning for automatic quadrilateral mesh generation: a soft actor-critic approach

Jie Pan<sup>a</sup>, Jingwei Huang<sup>b</sup>, Gengdong Cheng<sup>c</sup>, Yong Zeng<sup>a,\*</sup>

<sup>a</sup>*Concordia Institute for Information Systems Engineering, Concordia University, Montreal, H3G 1M8, Quebec, Canada*

<sup>b</sup>*Department of Engineering Management & Systems Engineering, Old Dominion University, Norfolk, 23529, Virginia, United States*

<sup>c</sup>*Department of Engineering Mechanics, Dalian University of Technology, Dalian, 116023, Liaoning, China*

---

## Abstract

This paper proposes, implements, and evaluates a Reinforcement Learning (RL) based computational framework for automatic mesh generation. Mesh generation, as one of six basic research directions identified in NASA Vision 2030, is an important area in computational geometry and plays a fundamental role in numerical simulations in the area of finite element analysis (FEA) and computational fluid dynamics (CFD). Existing mesh generation methods suffer from high computational complexity, low mesh quality in complex geometries, and speed limitations. By formulating the mesh generation as a Markov decision process (MDP) problem, we are able to use soft actor-critic, a state-of-the-art RL algorithm, to learn the meshing agent's policy from trials automatically, and achieve a fully automatic mesh generation system without human intervention and any extra clean-up operations, which are typically needed in current commercial software. In our experiments and comparison with a number of representative commercial software, our system demonstrates promising performance with respect to generalizability, robustness, and effectiveness.

*Keywords:* Reinforcement learning, mesh generation, soft actor-critic, neural networks, computational geometry, quadrilateral mesh

---



---

\*Corresponding author

*Email address:* yong.zeng@concordia.ca (Yong Zeng )

## 1. Introduction

Reinforcement learning (RL) has been flourished in many fields, such as games (Silver et al., 2016), healthcare (Gottesman et al., 2019), natural language processing (Wang et al., 2018b), and NP-hard problems (Mazyavkina et al., 2021). However, it is rarely applied to the area of computational geometry, especially in the field of mesh generation. Mesh generation is the fundamental step in conducting numerical simulations in the fields of finite element analysis (FEA), computational fluid dynamics (CFD), or graphic model rendering (Gordon and Hall, 1973; Roca and Loseille, 2019). Mesh generation techniques have been identified as one of the six basic research directions in NASA’s Vision 2030 CFD study (Slotnick et al., 2014). It discretizes complex geometric domains into a finite set of (geometrically simple and bounded) elements, such as triangles or quadrilaterals (in 2D geometries) or tetrahedra or hexahedron (in 3D geometries). Since the reliable automation and high quality of mesh representation matter significantly to the numerical simulation results, mesh generation has continued to be significant bottlenecks in those fields due to algorithm complexities, inadequate error estimation capabilities, and complex geometries (Slotnick et al., 2014). The rapid progress of deep learning and RL techniques offers the potential for mesh generation to have radical advances to overcome those challenges.

### 1.1. Mesh generation challenges

In most real-world engineering problems, the geometries to mesh have complex shapes and sizes; hence, unstructured meshes are preferred because of the robustness and efficiency in adaption (Bommers et al., 2013; Garimella et al., 2004; Owen, 1998). Quadrilateral elements of unstructured mesh can achieve more accurate numeral simulation results compared with triangular mesh (Verma and Suresh, 2017), which will be used in this paper. Conventional methods for quadrilateral mesh generation can be classified into two categories: indirect and direct methods (Shewchuk, 2012). Indirect methods start with a triangular mesh and then transform the triangular elements into quadrilateral elements by various strategies, including optimization (Brewer et al., 2003), refinement and coarsening (Garimella et al., 2004), simplification (Daniels et al., 2008), perfect matching (Remacle et al., 2012). These methods, however, suffer from a large number of irregular vertices, which is undesired in numerical simulations. Direct methods generate quadrilateral elements directly. These methods include 1) advancing front technique,

which recursively generates elements from the domain boundary and updates its boundary inwardly by cutting off generated elements until the whole domain is filled with quadrilateral elements (Zhu et al., 1991; Zeng and Cheng, 1993; Blacker and Stephenson, 1991; White and Kinney, 1997); 2) modifying the quadtree background grid to conform to the domain boundaries (Baehmann et al., 1987; Liang et al., 2010; Liang and Zhang, 2012; Atalay et al., 2008); 3) packing techniques, including square packing (Shimada et al., 1998) and circle packing (Bern and Eppstein, 2000); and template-based mapping methods (Cheng and Li, 1996). However, the generated quadrilateral meshes are usually not complete (e.g., containing triangular elements), having flat or inverted quadrilateral elements, and too much irregular arrangement. Therefore, a large amount of clean-up operations are implemented to improve the mesh quality. The strategies range from pre-processing, such as dividing complex geometries into small regular regions to facilitate generating regular mesh (Liu et al., 2017), to post-processing, such as reducing the singularity (Verma and Suresh, 2017), performing iterative topological changes (e.g., splitting, swapping, and collapsing elements) (Docampo-Sanchez and Haimes, 2019), and mesh adaptation (Verma and Suresh, 2018).

Therefore, many efforts have been made to improve meshing algorithms, including using heuristic clean-up operations to reduce the flat or inverted elements by re-adjusting location and connectivity of element vertices; using global and local remeshing techniques to reconstruct generated mesh in terms of topological and geometric features (Verma and Suresh, 2017); and pre-processing the geometry to ease the element generation process (Liu et al., 2017). Although the mesh quality has improved, the extra treatments make the meshing algorithms suffer from high complexity and speed limitations, and incur expensive trial-and-error tuning for researchers.

The aforementioned work names only a few recent advancements towards the automation of mesh generation. Although those extra treatments could achieve the high-quality, they bring in additional computational expense besides already complicated meshing algorithms and decrease the automation to some extent. Moreover, algorithm development is usually heuristic and requires human designers to search for knowledge in a time-consuming manner. It is urgent and necessary to build an efficient computational framework for mesh generation to sidestep the complexities and computational burden of existing meshing algorithms and relieve human algorithm designers from an inefficient and incomplete development of heuristic knowledge.

This framework should provide high-quality meshes for various complex geometries while maintaining adaptive automation, and avoiding any extra treatments.

### *1.2. Related work*

Machine learning techniques have been approved successfully to solve complex and time-consuming problems in various industrial areas. Researchers have started to combine mesh generation with artificial intelligence. Existing work can be classified into three kinds: 1) mesh optimization. Zhang et al. (2020) combined deep neural networks (NNs) with an external mesh generator to refine meshes with a better element distribution that can accurately solve Partial Differential Equations (PDE). Yang et al. (2021) trained a mesh refinement policy to dynamically adjust the mesh resolution for a better trade-off between simulation accuracy and computation cost via RL. 2) mesh reconstruction. Neural Mesh Flow (NMF) (Gupta, 2020) was a 3D mesh reconstruction method by deforming a template mesh into a target mesh using several Neural Ordinary Differential Equation (NODE, a deep neural network model (Chen et al., 2018)) blocks. NMF had its strength in the mesh property of manifoldness, which was beneficial for graphic rendering and 3D printing. Pixel2mesh (Wang et al., 2018a) was a deep learning architecture to produce 3D triangular mesh from a single RGB image. The generation process was a series of deformation from an ellipsoid with image perceptual features extracted by a convolutional neural network (CNN) to a target mesh model represented by a Graph Convolutional Network (GCN (Defferrard et al., 2016)). Wen et al. (2019) extended the Pixel2mesh for better shape quality from multi-view images. MeshCNN (Hanocka et al., 2019) was a NN architecture for simplifying meshes by specialized convolution and pooling operations that collapse edges. These recent advances show that mesh related works have gained significant attention in computational graphics and computer vision. 3) mesh generation. Nechaeva (2006) proposed an adaptive mesh generation algorithm based on self-organizing maps (SOM) (an unsupervised neural networks-based method), which adapts a given uniform mesh onto a target physical domain through mapping. The proposed method intended to overcome the drawbacks of SOM in tackling inaccurate mesh in the domain border and mesh construction for non-convex domains. Pointer networks (Vinyals et al., 2015), was a new neural architecture that aimed to solve combinatorial problems by NNs and could be used to generate triangular meshes by outputting a set of triplets of integers (each



forms a triangle) that correspond to the order of input points. The input contains both the points on the boundary and internal area of the geometry domain. As it is not designed for meshing problems, the final mesh is not robust and partially covered with triangular elements with even intersecting edges. Papagiannopoulos et al. (2021) proposed a triangular mesh generation method with three NNs. Given the training data derived from Constrained Delaunay Triangulation algorithm (Chew, 1989), three NNs could predict the number of candidate inner vertices (to form a triangular element), coordinates of those vertices, and their connection relations with existing segments on the boundary, respectively. Because of the fixed input size and complex network architectures, the method cannot adapt to arbitrary and complex geometry domains. Additionally, the resulting meshes are constrained by the quality and sample diversity of the selected training data, especially when it comes to geometries with complex boundary shapes.

Zeng and Cheng (1993) proposed a knowledge-based method, FreeMesh, to recursively extract quadrilateral elements following a domain boundary until the remaining boundary becomes a quadrilateral element, based on the recursive logic of design (Zeng and Cheng, 1991). Yao et al. (2005) improved the FreeMesh approach by introducing an artificial neural network (ANN) to learn the element extraction rules from a set of pre-selected samples of good quality quad meshes. Pan et al. (2021) built a self-learning automatic quadrilateral mesh generation system by combining a feedforward neural network (FNN) and an RL algorithm (Advantage Actor-Critic, A2C). The RL is used to provide high-quality samples to train an FNN model that serves as the final mesh generator to mesh various geometry domains. The resulting meshes outperform three conventional methods in two quality metrics. The shortcoming is that the training procedure is not fully automatic and requires extract operations from human designers, such as carefully designing the strategies to select samples for the FNN training in order to balance samples for applying rules in various situations.

Although many artificial intelligence (AI) techniques have started to be explored and applied to the field of mesh generation, a robust computational framework for mesh generation that can replace the standard mesh generation algorithms is still missing. With the rapid progressing of High Performance Computing (HPC), mesh generation algorithms will intuitively encounter tasks requiring higher resolution simulations, fast, and reliable processing, which could make conventional methods problematic. A new meshing algorithm that exploits both emerging HPC capabilities and ma-

chine learning/deep learning algorithms remains open exploration with great potential. In general, supervised NN-based methods rely on training data from existing conventional methods or handmade data, which cannot guarantee the overall quality and adapt to other domain boundaries; they have complex network structures, which increases the training difficulty; they are hard to apply to other domains with complex boundaries because of the fixed input size and generation strategies.

RL is a well-known self-taught learning paradigm for solving sequential decision making problems and has been successfully demonstrated in many fields. By formulating the mesh generation as a Markov decision process (MDP) (Pan et al., 2021), the meshing policy can be learned by the interactions between the agent and the environment without the need for supervised labels. Compared with most existing benchmark problems and complex applications of RL (Machado et al., 2018; Osband et al., 2019), the mesh generation problem poses new challenges for learning an optimal policy: 1) the environments (i.e., the geometries to mesh) have diverse shapes and sizes, which requires the policy to be adaptable and general; 2) the credit assignment for each time step to achieve the final mesh is difficult since the objective is not intuitive; 3) there is a trade-off between the immediate reward achieved by the current action and the future rewards that depend on the state of the environment caused by the current action, because the shape and size of the current generated element will shape the remaining boundary of the geometry to mesh. In the previous work (Pan et al., 2021), these challenges are not completely addressed by the RL algorithm, because its purpose is to generate samples for an FNN model rather than complete the mesh. Therefore, this article redesigns the state representation, action formulation, and reward function to fully automatically address those challenges. The new reward function could address the issues, including a) the trade-off between the current element quality and an overall mesh high quality and b) the completion of the mesh within finite steps. A novel RL technique, the soft actor-critic (SAC) method (Haarnoja et al., 2018a,b), is used to solve the learning of the meshing policy. SAC is one of the state-of-the-art off-policy learning algorithms and has faster learning efficiency and better stability in hyperparameters tuning than the A2C method.

The mesh generation problem also has the potential to study many RL topics, such as state representation and reward specification. Usually, the performance of newly invented or improved RL algorithms is evaluated crossing many benchmark problems (Mnih et al., 2013). However, these bench-

mark problems have some limitations: 1) the internal dynamic mechanisms of different problems may impact the performance and hardly provide accurate evaluation for RL methods, especially complex problems (Berner et al., 2019; Vinyals et al., 2017); 2) the state representations are different across different problems, which may hinder the algorithm analysis; 3) some of the problems are simple, and the reward function is relatively simple (i.e., game scores (Mnih et al., 2013)), which cannot study the reward specification in-depth. The challenges of the mesh generation problem enable it to be a potential benchmark problem for understanding many RL issues. The diverse environments can be used to test the scalability and generality of the learned policy; the range of agent’s observation can be easily adjusted and used to study the partial MDP; the reward designing can be used for testing exploration and credit assignment problems.

### *1.3. Contributions*

In this paper, we propose, implement, and evaluate an RL based fully automatic mesh generation system. The main contributions of this paper are summarized as follows.

1. The proposed RL-based automatic mesh generation system achieves a level of fully automatic mesh generation without human intervention and any extra clean-up operations, which are typically needed in current commercial software.
2. In our experiments and comparison with a number of representative commercial software, our system demonstrates competitive performance in several aspects, including mesh regularity, high quality in various geometry domains, and the necessity of handling not expected elements (i.e., triangles).
3. Our experiments demonstrate an interesting approach to achieving generalizability and scalability compared with many RL applications by using partial observation of the environment.

The rest of the paper is organized as follows. Section 2 presents the formulation of the mesh generation problem into an MDP problem and fundamental components. Section 3 introduces the detailed implementation of SAC for mesh generation. Section 4 evaluates the performance of the proposed method and compares with other state-of-the-art meshing approaches. Section 5 discusses the important improvements of the proposed method to

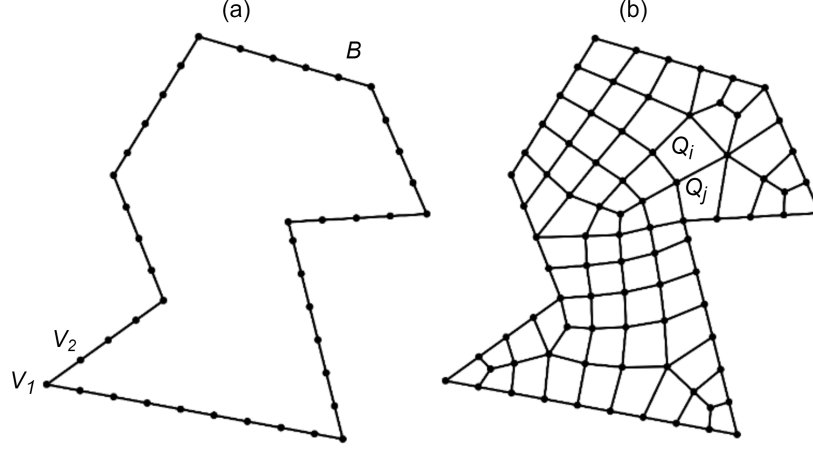


Figure 1: Meshing problem. (a) The initial geometry is defined by the boundary  $B$  consisting of a set of vertices  $V$ ; (b) The final mesh is the result of discretization into a set of quadrilateral elements  $Q$ .

mesh generation and RL communities. Section 6 concludes this article and indicates some future directions.

## 2. Problem formulation and fundamentals

In this section, the formulation of mesh generation as an MDP problem and related RL techniques are introduced.

### 2.1. Problem formulation

The problem of non-simplicial mesh generation (i.e. quadrilaterals) in single-connected 2D domains is studied. The purpose of mesh generation is to discretize a geometric domain (see Fig. 1(a)) into quadrilateral elements (see Fig. 1(b)). The boundary of the domain,  $B$ , is composed of piecewise linear segments and is then represented as a sequence of vertices  $[V_1, V_2, \dots, V_N]$ . The final mesh,  $\Omega$ , is composed of a set of quadrilateral elements  $[Q_1, Q_2, \dots, Q_M]$ . Consequently, a mesh should satisfy: 1) each element is a quadrilateral; (2) the inner corner of each element should be between  $45^\circ$  and  $135^\circ$ ; (3) the aspect ratio (the ratio of opposite edges) and taper ratio (the ratio of neighbouring edges) of each quadrilateral should be within a predefined range; (4) the transition between a dense mesh and a coarse mesh should be smooth (Zeng and Cheng, 1993; Zeng and Yao, 2009).

In the previous work, the meshing problem is preliminarily formulated as an RL problem (Pan et al., 2021). The mesh generation problem can be seen as a control problem with a sequence of steps to generate mesh elements. As illustrated in Fig. 2, quadrilateral elements can be generated one by one, starting from the boundary of the domain and updating its boundary inwardly by removing the generated element, until there are only four vertices left in the updated boundary, which forms the last element. This procedure can be discretized into four steps: 1) choosing a vertex (called reference vertex in this paper) from the boundary; 2) constructing an element around the reference vertex; 3) removing the generated element, and; 4) updating the boundary. The meshing boundaries are continuously shaped by the generated elements. In each iteration, the meshing problem is evolved and depends on the previous solution (i.e., the mesh element) of the previous problem, which forms a sequential decision making process, also called an MDP. The quality of future elements hinges on the shape and size of the previously generated elements. Usually, when the updated boundary is approaching itself, the quality of the element will start to drop, or even elements meeting the requirements cannot be constructed.

In this formal framework, the meshing boundary is considered as the environment, in which the agent generates quadrilateral elements using a set of actions. The goal of the agent is to complete the mesh given any geometric objects, which satisfies the requirement mentioned above. The overall architecture is shown in Fig. 3. The agent, at each time step  $t$ , observes a state  $S_t$  from the environment, and conducts an action  $A_t$  applied to the environment. The environment responds to the action and transits into a new state  $S_{t+1}$ . It then reveals the new state and provides a reward  $R_t$  to the agent. This process forms an iteration and repeats until a given condition is satisfied (i.e., the RL problem is solved).

The main problem in the previous method is that the procedure to obtain the final mesh agent is complex and involves three phases: RL-based sampling, experience extraction, and FNN training. It is not a fully automatic method and requires extract operations from human designers, such as carefully designing the strategies to select samples because the imbalanced samples will hinder the final performance.

To overcome this problem and reduce the extra operations, an automatic mesh generation method based solely on RL is proposed in this paper. The meshing policy is self-learned from the interactions between the RL agent and the environment through trial-and-error. The learned policy could adapt to

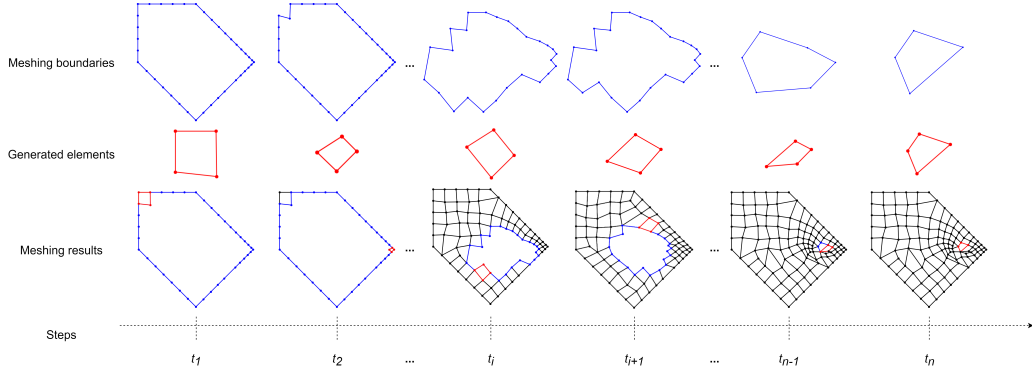


Figure 2: A sequence of actions taken by the mesh generator to complete a mesh. At each time step  $t_i$ , an element (in red) is extracted from the current boundary (in blue). The boundary is then updated by cutting off the element and serves as the meshing boundary in the next time step  $t_{i+1}$ . This process continues until the updated boundary becomes an element.

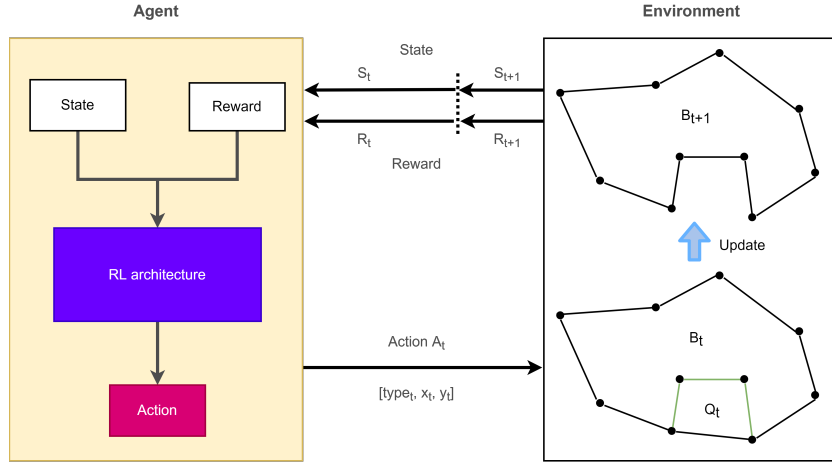


Figure 3: The RL-based computational framework for automatic mesh generation. The agent is the mesh generator that could implement various RL techniques. It generates an element at a time by the action. The environment represents the meshing boundary and updates the boundary once an element is produced.

any geometric domain because a partial boundary is adopted as the state representation instead of the whole boundary. Compared with most existing methods, this method is computationally efficient and does not need any extra operations after meshing a geometry. The mesh quality requirement is embedded in the reward function, which measures how well each element generated at each step is contributed to the final mesh. Additionally, the reward function can be customized or controlled by the down-streaming applications to meet their specific quality requirements, such as sparse or dense density. By controlling the reward function, it is a straightforward pathway to acquire needed mesh and avoids many time-consuming and computationally complex post-processing operations (e.g., clean-up and remeshing).

## 2.2. Reinforcement learning

In many RL applications, the policies have a fixed size of the input state and are applicable to environments that are similar to the training environment. For instance, Wei et al. (2020) trained different models for elevator settings.

RL is a learning paradigm that has been used to address a sequential decision making problem, mathematically known as an MDP problem. The technique is to enable an agent to learn from the interactions with its environment by trial-and-error via reward feedback from its actions and experiences (Kaelbling et al., 1996; Sutton and Barto, 2018). Eventually, a policy will be learned by the agent for guiding appropriately selecting actions under each environmental situation over time to maximize the accumulated reward. According to different learning objectives, the policy could be learned in a direct (policy-based) or indirect (value-function-based) fashion.

Value-function-based methods estimate the expected reward for the agent to start from a state or to perform a given action in a given state. The optimal policy can be implicitly derived from the optimal value function. Deep Q-Network (DQN) is a recent breakthrough in estimating value function via a deep neural network (Mnih et al., 2013), which stabilizes the training of action value function using experience replay and target network and generalizes a framework for end-to-end RL tasks using the same algorithm. Many successors are continuously improving DQN from various aspects, e.g., asynchronous advantage actor-critic (A3C) (Mnih et al., 2016), dueling network to better estimate action value function (Wang et al., 2016), and combating sparse reward issues by Hindsight Experience Replay (HER) (Andrychowicz et al., 2017). For the mesh generation problem, the action is continuous and

requires choosing appropriate points to form an element from an area. Correspondingly, the meshing environment will be altered and evolved into various shapes after each action. Hence, to discretize both state and action spaces may distort the feedback regarding the impact of the agent’s actions on the environment and adversely hinders exploring feasible action space, causing a sub-optimal policy.

Policy-based methods directly estimate a policy to guide the agent to choose actions under various environmental states. The policy is usually modelled by a parameterized function. The modern policy-based methods have several divisions, including Deep Deterministic Policy Gradient (DDPG) (Lillicrap et al., 2015) using policy gradient, A3C (Mnih et al., 2016) combining actor and critic together, Proximal Policy Optimization (PPO) (Schulman et al., 2017) via trust region, TD3 (Fujimoto et al., 2018) improving DDPG by considering function approximation error, and SAC (Haarnoja et al., 2018a,b) with off-policy learning.

RL methods have been gradually applied to many applications in various areas and achieved promising performance (Li, 2018). Since the mesh generation problem can be cast as an MDP problem, it is intriguing to solve the problem by RL. Formally, the MDP has a set of states  $S$ , a set of actions  $A(s)$  for a given state  $s$ , and a reward function  $R$ . Their formulation is altered and improved from the previous method to align the new objective, completing the mesh rather than providing training samples. The detailed definition will be explained in the next section.

Since the stability, robustness, and efficiency of meshing algorithms are critical for down-streaming applications, a customized RL algorithm, SAC, is used in this article. SAC is one of the state-of-the-art policy-based algorithms and has advantages in better sample efficiency and stable convergence. The hypothesis behind RL is that all the goals can be represented by the maximization of the expected cumulative reward. In this article, a well designed reward function will guide the policy learning to accomplish the meshing task. The RL-based computational framework for mesh generation offers a direct solution to acquire the mesh satisfying the quality requirement; it provides a pathway to customize the ideal mesh for down-streaming applications by adjusting the reward function; and it is a fully automatic method for various complex geometry domains without extra clean-up treatments.



### 3. RL based mesh generation

In this section, a self-learning computational framework for automatic mesh generation via RL is proposed. Quadrilateral element generation in single-connected 2D domains is used as an example to demonstrate this method. The action formulation and state representation of the problem is described first. Then, the reward function is defined. Finally, the detailed implementation of SAC is explained.

#### 3.1. Action formulation

In this formal framework, the agent will take actions to generate an element at each time step according to the current boundary. The search for the best action includes 1) how to choose the reference vertex? And 2) how to decide the other three vertices to construct an element?

For the first question, the general principle to select a vertex is the least averaged boundary angle first, which is to avoid creating hard boundary situations for the subsequent actions. The vertex will be the reference vertex  $V_i^*$  when it forms the least angle with its surrounding vertices, as denoted by

$$V_i^* = \arg \min_{V_i} \frac{1}{n_{rv}} \sum_{j=1}^{n_{rv}} \angle V_{l,j} V_i V_{r,j} \quad (1)$$

where  $V_{l,j}$  and  $V_{r,j}$  denote the  $j$ -th vertices at the left and right side (considering clockwise orientation) of the reference vertex  $V_i$  along the boundary, respectively;  $n_{rv}$  represents how many surrounding vertices should be included, which  $n_{rv} = 2$  is used in this article;  $V_i$  is the  $i$ -th vertex on the boundary. Since this strategy is consistent across all the actions, the reference vertex selection is automatically implemented by the environment rather than by the agent.

For the second question, once the reference vertex is determined, there are three kinds of basic situations to form an element: adding zero, one, or two vertices (Zeng and Cheng, 1993). Therefore, as shown in Fig. 4, the action is formally defined as  $[type, V_1, V_2]$ , where  $type \in \{0, 1, 2\}$ , which are corresponding to the three situations respectively;  $V_1$  and  $V_2$  are the coordinates of the newly added vertices. The coordinates space for the vertices are constrained to a fan-shaped area (in light blue) with radius  $r$ , which is calculated as follows:

$$\begin{aligned}
r &= \alpha * L, \\
L &= \frac{1}{2n} \sum_{i=0}^n |V_{l,i}V_{l,i+1}| + |V_{r,i}V_{r,i+1}|, 0 < n < N/2
\end{aligned} \tag{2}$$

where  $V_{l,i}$  and  $V_{r,i}$  denote the  $i$ -th vertex at the left and right side of the reference vertex along the boundary;  $V_{l,0} = V_{r,0}$  is the reference vertex;  $|V_*V_*|$  is the Euclidean distance between two vertices. We set  $\alpha = 1.5$  and  $n = 2$  in all our experiments. Usually, type 2 is only needed on special occasions, such as circular domains, and is operated at a constant level. Hence, to reduce the learning complexity, the action  $[type, V_1]$  is finally used in the experiments.

### 3.2. State representation

The state is the observation of the agent to the environment. The environment in mesh generation is the meshing boundary (see Fig. 2). The full state of the environment at time  $t$  would consist of all the vertices of the boundary. However, not all the vertices are meaningful and necessary to represent the environment. To adapt to all kinds of geometries, the inclusion of all vertices is also not a good option. Therefore, a partial observation of the boundary environment is considered, which includes the following components: a reference vertex determining where the agent should generate an element around, and its surrounding vertices providing a local environmental situation.

The state is denoted as  $s_t$ , and composed of five components (1) a reference vertex,  $V_0$ , which is used as the relative origin to generate the new element with a action  $a_t$ , and is calculated by iterating all the vertices on the boundary, computing the angle of each vertex formed by its left and right connected vertices, and selecting the vertex having the least angle; (2)  $n$  neighboring vertices on the right side of the reference vertex; (3)  $n$  neighboring vertices on the left side; (4)  $g$  neighboring points  $V_{\theta_1}, \dots, V_{\theta_g}$  in the fan-shaped area  $\theta_1, \dots, \theta_g$  with radius  $L_r$ , as shown in Fig. 5 ( $g = 3$ ), where  $\theta_1 = \theta_2 = \theta_3$ ;  $L_r = \beta * L$ . If there are no vertices in the fan-shaped area (e.g.,  $\theta_3$ ), the furthest bisector vertex in the area or the intersection vertex between the bisector and the boundary edge is selected, such as  $V_{\theta_3}$  in Fig. 5; (5)  $\rho_t$ , the area ratio between the updated domain and the original domain, which is used to indicate the meshing progress.

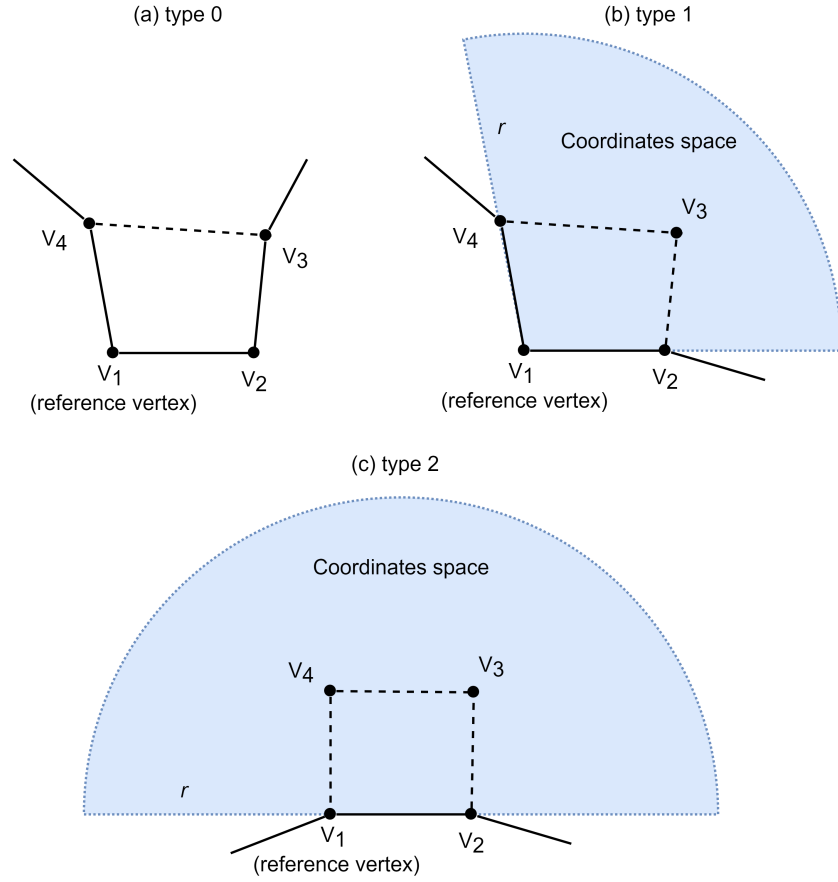


Figure 4: Action space for each rule type. Subfigures (a)-(c) correspond to three types of actions, respectively. The blue area is the space to select the candidate vertices, including  $V_3$  in type 1, and  $V_3$  and  $V_4$  in type 2, with the reference vertex  $V_1$  as the origin and a radius  $r$ .

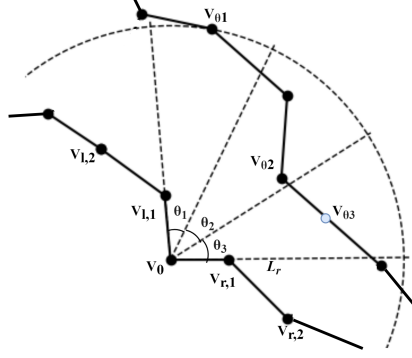


Figure 5: Partial observation of the meshing boundary. For example, the partial boundary, where  $L_r = 4, n = 2, g = 3$ , is represented as the state. First, two vertices on the left and right sides of the reference vertex  $V_0$  are selected, respectively. Second, the angle  $\angle V_{l,1}V_0V_{r,1}$  is evenly split into three angles  $\theta_1, \theta_2$ , and  $\theta_3$ ; three fan-shaped areas are hence formed with these angles and a radius  $L_r$ . Then, the closest vertex in each area is selected.  $V_{\theta_3}$  is an intersection vertex between the bisector and the boundary segment.

This partial boundary is arranged as follows:

$$S_t = \{V_{l,n}, \dots, V_{l,1}, V_{r,1}, \dots, V_{r,n}, V_{\theta_1}, \dots, V_{\theta_g}, \rho_t\}. \quad (3)$$

All the vertices are represented by a polar coordinates system with  $V_0$  as the origin and  $\overrightarrow{V_0V_{r,1}}$  as the reference direction. Since the x and y coordinates of the vertex  $V_0$  are both 0, it can be removed from the state representation. This representation only keeps the relative information among all the vertices.

### 3.3. Reward function

The reward function represents the objective of mesh generation, which is to achieve overall high mesh quality and completeness with finite elements. This is a stepwise reward signal that measures the performance of each action. There are three main cases in total: 1) if the action forms an invalid element or has intersections with the boundary edges, the reward is set to -0.1; 2) if the action forms the last element, the reward is set to 10; 3) if it generates a valid element, the reward is the joint measurement of element quality, the quality of the remaining boundary, and the density factor. Finally, the reward function is formally defined as follows:

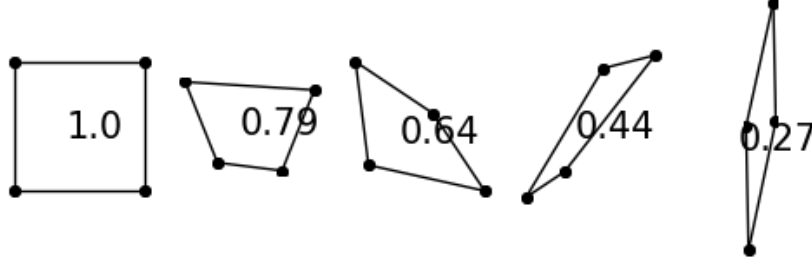


Figure 6: Element quality varies with different shapes. The quality value ranges from 0 to 1. The element with the best quality 1 is a square.

$$r_t(s_t, a_t) = \begin{cases} -0.1, & \text{invalid element;} \\ 10, & \text{the element is the last element;} \\ m_t, & \text{otherwise.} \end{cases} \quad (4)$$

The measurement  $m_t$  is calculated by the following equation:

$$m_t = \eta_t^e + \eta_t^b + \mu_t. \quad (5)$$

The element quality  $\eta_t^e$  is measured by its edges and internal angles situations, and is calculated as follows,

$$\begin{aligned} \eta_t^e &= \sqrt{q^{edge} q^{angle}}, \\ q^{edge} &= \frac{\sqrt{2} \min_{j \in \{0,1,2,3\}} \{l_j\}}{D_{max}}, \\ q^{angle} &= \frac{\min_{j \in \{0,1,2,3\}} \{angle_j\}}{\max_{j \in \{0,1,2,3\}} \{angle_j\}}, \end{aligned} \quad (6)$$

where  $q^{edge}$  refers to the quality of edges of this element;  $l_j$  is the length of the  $j$ th edge of the element;  $D_{max}$  is the length of the longest diagonal of the  $t$ th element;  $q^{angle}$  refers to the quality of the angles of the element; and  $angle_j$  is the degree of  $j$ th inner angle of the element. The quality  $\eta_t^e$  will range from 0 to 1, which is better if greater. Examples of various element qualities are shown in Fig. 6.

The quality of the remaining boundary is measured by both the quality of the angles formed between the newly generated elements and the boundary,

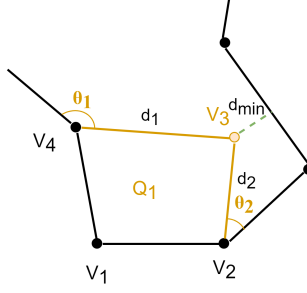


Figure 7: The quality of the remaining boundary.  $Q_1$  is the newly generated element. Once it is removed, it forms two angles  $\theta_1$  and  $\theta_2$  with existing boundary segments. The quality is jointly measured by these two angles, and the closest Euclidean distance  $d_{min}$  of the newly added vertex  $V_3$  is to the existing segments.  $d_1$  and  $d_2$  are the Euclidean lengths of segments  $V_3V_4$  and  $V_2V_3$ .

and the shortest distance of the generated vertex to its surrounding edges, and denoted as follows,

$$\eta_t^b = \sqrt{\frac{\min_{k \in \{0,1\}} \{\min(\theta_k, M_{angle})\}}{M_{angle}}} q^{dist} - 1, \quad (7)$$

$$q^{dist} = \begin{cases} \frac{d_{min}}{(d_1 + d_2)/2}, & \text{if } d_{min} < (d_1 + d_2)/2; \\ 1, & \text{otherwise.} \end{cases}$$

where  $\theta_k$  refers to the degree of the  $k$ th generated angle;  $d_{min}$  is the distance of  $V_3$  to its closet edges. The details are shown in Fig. 7. The quality  $\eta_t^b$  ranges from -1 to 0, which the larger value is the better quality. It serves as a penalty term to decrease the reward if the quality of the remaining boundary is getting worse. We set  $M_{angle} = 60$ . When the formed new angles are less than  $M_{angle}$ , the quality will decrease, which prevents the generation of sharp angles that are harmful to the overall mesh quality and may even fail the meshing process.

These two qualities together represent the trade-off between the generated element and the remaining boundary, which is critical to guarantee the overall mesh quality and completeness of the final mesh. The last term is a density factor  $\mu$ , which controls the mesh density and assure the meshing process will be completed in finite steps, and is calculated as follows,

$$\mu_t = \begin{cases} -1, & \text{if } \mathcal{A}_t < \mathcal{A}_{min}; \\ \frac{\mathcal{A}_t - \mathcal{A}_{min}}{\mathcal{A}_{max} - \mathcal{A}_{min}}, & \text{if } \mathcal{A}_{min} \leq \mathcal{A}_t < \mathcal{A}_{max} - 1; \\ 0, & \text{otherwise.} \end{cases} \quad (8)$$

where  $\mathcal{A}_t$  is the area of the element at time  $t$ ;  $\mathcal{A}_{min}$  is the estimated minimum area of the element that is tolerable to the meshing domain, and calculated by  $\mathcal{A}_{min} = v e_{min}^2$ ;  $\mathcal{A}_{max}$  is the estimated maximum area of the element, and calculated by  $\mathcal{A}_{max} = v \left( \frac{e_{max} - e_{min}}{\kappa} + e_{min} \right)^2$ ;  $e_{max}$  and  $e_{min}$  is the length of the longest and shortest edges in the boundary respectively;  $\kappa$  controls when to start the penalty and  $\kappa = 4$  in our experiment;  $v$  is a weight and ranges from  $[0, +\infty)$ , which the smaller value means the denser density, and vice versa. We set  $v = 1$  in our experiments for the medium density.

#### 3.4. Meshing scheme via SAC

The computational framework of mesh generation is based on the SAC approach. SAC is one of the state-of-the-art RL algorithms for continuous action control problems (Haarnoja et al., 2018a,b). To overcome the sample complexity and hyperparameter sensitivity, it adds an entropy item in addition to reward in the objective function, and maximizes the reward return while maximizing the randomness of the policy.

The objective function of the policy is correspondingly denoted as

$$J(\pi) = \sum_{t=1}^T \mathbb{E}_{(s_t, a_t) \sim \rho_{\pi_\theta}} [r(s_t, a_t) + \alpha \mathcal{H}(\pi_\theta(\cdot | s_t))], \quad (9)$$

where  $\mathcal{H}(\cdot)$  is the entropy measure (Ziebart, 2010);  $\rho_{\pi_\theta}$  is the state-action marginal distribution of policy  $\pi$  parameterized by  $\theta$ ;  $\alpha$  indicates the significance of the entropy item, known as temperature parameter. With considering the entropy maximization, it allows the learned policy acts as randomly as possible while guaranteeing task completion, which gains the trade-off of the exploration-exploitation and thus accelerates the learning. This randomness is especially important for partially observable environment.

For learning an optimal maximum entropy policy, SAC drives from the policy iteration method in the maximum entropy framework. During the policy evaluation step, the soft Q-value can be computed iteratively and defined as

$$Q(s_t, a_t) = r(s_t, a_t) + \gamma \mathbb{E}_{s_{t+1} \sim \rho_\pi(s)}[V(s_{t+1})], \quad (10)$$

where

$$V(s_t) = \mathbb{E}_{a_t \sim \pi}[Q(s_t, a_t) - \alpha \log \pi(a_t|s_t)], \quad (11)$$

where  $\rho_\pi(s)$  and  $\rho_\pi(s, a)$  are the state and the state-action marginals of the trajectory distribution induced by a policy  $\pi(a_t|s_t)$ . The soft Q-function  $Q_\theta(s_t, a_t)$  is parameterized by a neural network with parameters  $\theta$ . The soft state value function  $V(s_t)$  is implicitly parameterized by the soft Q-function parameters. To update the soft Q-function, its gradient is estimated by the formula,

$$\hat{\nabla}_\theta J_Q(\theta) = \nabla_\theta Q_\theta(s_t, a_t)(Q_\theta(s_t, a_t) - (r(s_t, a_t) + \gamma(Q_{\bar{\theta}}(s_{t+1}, a_{t+1}) - \alpha \log(\pi_\phi(a_{t+1}|s_{t+1}))))), \quad (12)$$

where  $\pi_\phi$  is the current policy parameterized by a neural network with parameter  $\phi$ ;  $\bar{\theta}$  is obtained as an exponential moving average of the soft Q-function network weights.

In the soft policy improvement stage, the policy parameter can be updated by minimizing the expected KL-divergence,

$$J(\phi) = \mathbb{E}_{s_t \sim \mathcal{D}}[\mathbb{E}_{a_t \sim \pi_\phi}[\alpha \log(\pi_\phi(a_t|s_t)) - Q_\theta(s_t, a_t)]]. \quad (13)$$

Its gradient can be approximated by

$$\hat{\nabla}_\phi J_\pi(\phi) = \nabla_\phi \alpha \log(\pi_\phi(a_t|s_t)) + (\nabla_{a_t} \alpha \log(\pi_\phi(a_t|s_t)) - \nabla_{a_t} Q(s_t, a_t)) \nabla_\phi f_\phi(\epsilon_t; s_t), \quad (14)$$

where  $\epsilon_t$  is an input noise vector and can be sampled from some fixed distribution;  $f_\phi(\epsilon_t; s_t)$  is a reparameterized policy using a neural network transformation.

Finally, the temperature  $\alpha$  is updated by minimizing the objective

$$J(\alpha) = \mathbb{E}_{a_t \sim \pi}[-\alpha \log \pi_\phi(a_t|s) - \alpha \bar{\mathcal{H}}]. \quad (15)$$

The details of the algorithm are shown as Algorithm 1.



---

**Algorithm 1** SAC for mesh generation.

---

```
1: initialize network parameters  $\theta_1, \theta_2$  and  $\phi$ 
2:  $\bar{\theta}_1 \leftarrow \theta_1, \bar{\theta}_2 \leftarrow \theta_2$ 
3: for each episode do
4:   for each time step do
5:     Select action  $a_t \sim \pi_\phi(\cdot|s_t)$ 
6:     Observe reward  $r$  and new state  $s'$ 
7:     Store  $(s_t, a_t, r_t, s_{t+1})$  in replay buffer  $\mathcal{D}$ 
8:   end for
9:   for each gradient step do
10:    Sample  $m$  batches from replay buffer
11:    Update soft Q-function  $\theta_i \leftarrow \theta_i - \lambda_Q \hat{\nabla}_{\theta_i} J_Q(\theta_i)$  for  $i \in \{1, 2\}$ 
12:    Update policy network  $\phi \leftarrow \phi - \lambda_\pi \hat{\nabla}_\phi J_\pi(\phi)$ 
13:    Update target network  $\bar{\theta}_i \leftarrow \tau\theta_i + (1 - \tau)\bar{\theta}_i$  for  $i \in \{1, 2\}$ 
14:    Adjust temperature  $\alpha \leftarrow \alpha - \lambda \nabla_\alpha J(\alpha)$ 
15:   end for
16: end for
```

---

#### 4. Experimental results

In this section, the effectiveness of the proposed method, FreeMesh-RL, will be evaluated by a few types of experiments: scalability verification and meshing performance comparison. Since the scalability challenge is common for NN-based meshing methods and RL-based applications, we will evaluate the FreeMesh-RL method over different complex domains or the same domain with different scales on size. The second type of experiment is to compare the meshing performance of FreeMesh-RL with two start-of-the-art meshing approaches over three predefined geometry domains. To obtain optimal meshing performance, we also examine the impact of different RL algorithms, training domains, observation, and reward function on the learning of the policy.

To the best of our knowledge, there is no baseline environment of mesh generation in the RL field. We build a simulation environment with Python and PyTorch, which will be cleaned up and opened for the community to test various RL algorithms in the future.

#### 4.1. Implementation details

This section examines the optimal RL method for mesh generation, the selection of training domains, details the training of SAC method, and discusses the design of state representation and reward function. All the experiments are conducted on a computer with an i7-8700 CPU and an Nvidia GTX 1080 Ti GPU with 32 GB of RAM. A total of 1.2 million time steps are adopted for the policy training.

##### 4.1.1. RL methods comparison

We have compared the learning efficiency of 4 kinds of RL algorithms (i.e., PPO, DDPG, TD3, and SAC) over the same training domain. Their hyperparameters use the standard settings (Raffin et al., 2021). The comparison results are shown in Fig. 8. In the early stage of training ( $< 5e4$ ), DDPG, TD3, and SAC achieve faster learning performance than the PPO method. Then DDPG and TD3 slow down the learning pace, but SAC maintains the high learning speed and converges to a stable meshing policy. PPO gradually achieves suboptimal performance, but the learning process is not steady. Without further hyperparameters adjustment, the SAC method can fast converge to a stable meshing policy, making it the optimal method for mesh generation.

##### 4.1.2. Training domain selection

A training domain is needed for the RL method to learn the meshing policy. In a real engineering environment, the meshing domains have diverse shapes and topological structures. Generally, the domain boundary features include sharp angles, bottleneck regions, and unevenly distributed boundary segments in a single connected 2D geometry. Therefore, the training domain can have any shape but has to meet those criteria to ensure the richness of samples. Since the meshing process in this paper is element-wise, the meshing boundary will be continuously changed with the generation of elements and evolve into various shapes, enriching the sample diversity, as shown in Fig. 2. The total number of evolved boundaries is equivalent to how many elements generated.

We have designed three candidate domains based on the criteria, T1, T2, and T3, as shown in Fig. 9(a-c). The training results over them using SAC are shown in Fig. 9(d). Both domain T1 and T2 achieve fast learning speed and converge to a stable meshing policy, but T1 has less learning fluctuation. The agent spends more time learning to mesh Domain T3 because of

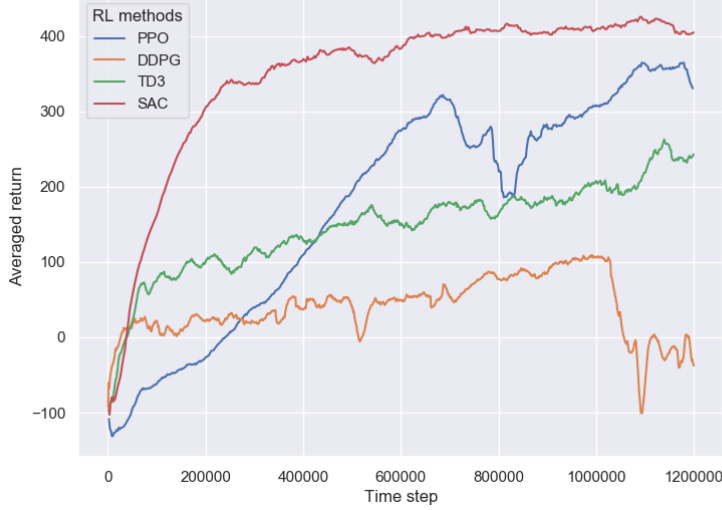


Figure 8: Learning efficiency comparison of various RL algorithms. Four kinds of RL algorithms, PPO, DDPG, TD3, and SAC, are chosen to compare the learning efficiency over the same training domain. A total of 1.2 million time steps are executed.

multiple shape angles. The learned policy is also not stable as the other two domains have learned. Since a robust policy matters to the meshing performance, domain T1 is chosen as the sole training domain to obtain the final meshing policy. Specifically, the trained policy will mesh other unseen domain boundaries for performance evaluation experiments without additional training.

#### 4.1.3. SAC training

We have examined the learning performance of different neural network architectures in SAC. The comparison results are shown in Fig. 10(a). The NN structure S1 has the poorest performance in learning the policy. The network architecture with three hidden layers,  $[128, 128, 128]$  (i.e., S2), achieves best learning performance while having fewer parameters compared with S3 and S4, which is selected in this work to approximate the soft Q-function, policy, and target networks.

Random seeds usually affect the learning performance. We select three different random seeds and test their impact on the policy learning, as shown in Fig. 10(b). It turns out that the SAC’s learning process is not sensitive to

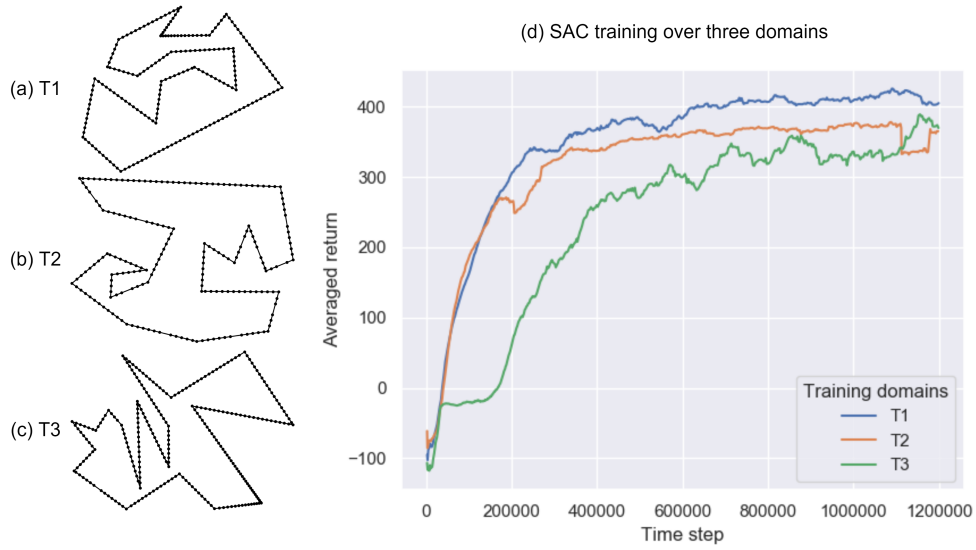


Figure 9: Learning difficulty comparison over different training domains. (a)-(c) three kinds of training domains, T1, T2, and T3, are designed based on the identified criteria. (d) The training results over three domains using SAC. Domain T1 achieves the fast and stable learning efficiency which is easier to learn a meshing policy than the other two domains, whereas Domain T3 is the hardest one to converge to a stable policy because multiple sharp angles exist.

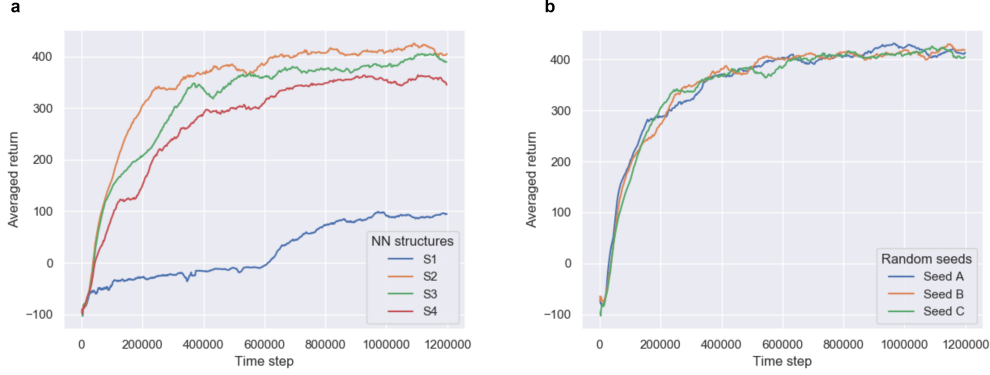


Figure 10: Comparisons of neural network structures and random seeds for the SAC method. (a) NN structures comparison: S1-4 represent four different neural network structures in the hidden layers, including [32, 32], [128, 128, 128], [64, 64, 64, 64, 64], and [32, 128, 128, 128, 64, 32], respectively. NN structure S2 achieves the fast and stable learning result. (b) Random seeds comparison: three different random seeds, A (356), B (567), and C (999), are chosen to examine the learning difference. Certainly, SAC is not sensitive to those random seeds and could achieve stable learning results.

those seeds, which is one of the advantages compared with other RL methods. The other hyperparameters used for SAC are listed in the Table 1.

Table 1: Training hyperparameters for SAC algorithm.

Parameter	Description	Value
$N_{\mathcal{D}}$	Experience pool size	1e6
$m$	Minibatch size	256
$\gamma$	Discount factor	0.99
$\lambda_Q, \lambda_\pi$	Learning rate	3e-4
$\tau$	Soft update factor	5e-3

#### 4.1.4. Agent’s view of environmental state

The state is the agent’s observation from the environment, which will significantly influence the agent’s decision making. Since the partial observation is adopted in the proposed method, We need to decide how much is appropriate and effective to be observed by the agent to learn the meshing policy. The range of the observation is controlled by three factors,  $L_r, n$

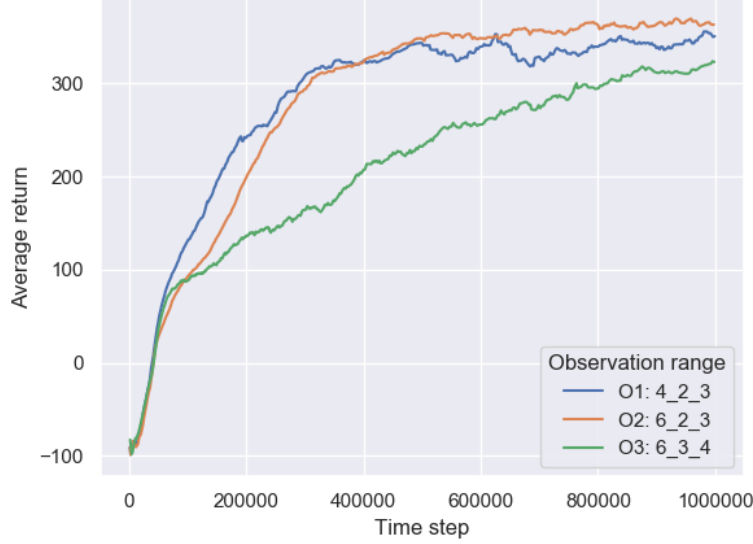


Figure 11: Learning efficiency comparison of different agent’s observation ranges. The observation range is formed by  $L_r\_n\_g$ , which represents the radius of the fan shape in the state, the number of neighbouring vertices on the left and right side of the reference vertex, and the number of vertices in the fan-shaped area, respectively. This range determines how far and how much information the agent will be observed from the meshing environment.

and  $g$ , in Equation 3. The factor  $L_r$  controls how far the agent can observe from its position while the other two factors determine how many vertices the agent perceives around the reference vertex. The leaning performance is compared with three kinds of settings,  $O1$  ( $L_r = 4, n = 2, g = 3$ ),  $O2$  ( $L_r = 6, n = 2, g = 3$ ), and  $O3$  ( $L_r = 6, n = 3, g = 4$ ). The comparison results are shown in Fig. 11. By comparing  $O1$  and  $O2$ , it can be found that further observation contributes to more return. This is because the agent could adjust the position of the candidate vertex in advance to avoid a conflict with the remaining boundary. Meanwhile, since the chance of noticing vertices in the fan-shaped area will be increased, the more complex information will be included in the state, which the learning speed may become slower in the earlier stage. A similar phenomenon can be observed when comparing  $O2$  and  $O3$ . The more information the agent observes, the more time to build the correlation is needed. In this paper, the observation  $O2$  is hence used as the state representation across all the experiments.

#### 4.1.5. Reward function

The reward function represents the objective of mesh generation, which mainly consists of overall high mesh quality and completeness with finite elements. There are three terms in the reward function, element quality  $\eta_t^e$ , the quality of remaining boundary  $\eta_t^b$ , and density factor  $\mu_t$ , which guides the policy learning to fulfill the objective. The first two terms guarantee the mesh quality and the easiness of continuing meshing. The last term controls the meshing density by the factor  $v$  that can adjust the minimum tolerant element size, and assure the mesh termination within finite steps. Since the first two terms are necessary for the overall mesh quality, they cannot be easily changed if the quality requirement is predefined, whereas the third term is controllable. Three kinds of density are thus compared, including sparse ( $v = 1.5$ ), medium ( $v = 1$ ), and dense ( $v = 0.5$ ) settings. The comparison results are shown in Fig. 12(a)-(c). We also examine the number of elements for each density after running 10 episodes, as shown in Fig. 12(d). The difference in the average number of elements between sparse and medium is about 20 elements, while the difference between medium and dense density is around 50 in this testing domain boundary. The medium density is used across all the remaining experiments.

#### 4.2. Evaluation

The mechanisms of a few NN-based mesh generation methods are qualitatively analyzed. The effectiveness of the proposed FreeMesh-RL is then measured in two aspects: scalability and meshing performance. All the meshing results are derived from the same model trained on the domain T1 (see Fig. 9(a)).

##### 4.2.1. Comparison to NN-based methods

The automation level and mesh quality are the two most important properties in mesh generation methods. We have compared some popular NN-based mesh generation methods with FreeMesh-RL from the perspective of the learning method, as shown in Table 2. The methods proposed by Papiannopoulos et al. (2021) and Yao et al. (2005) use FNN to estimate the mapping relation between the geometry and the mesh, and require a large amount of labelled data, either from existing meshing tools (e.g., Gmsh (Geuzaine and Remacle, 2009)), or handcrafted samples. However, it is difficult to guarantee the completeness and balance of obtained data, which will comprise the meshing performance significantly. Pan et al. (2021) intends to

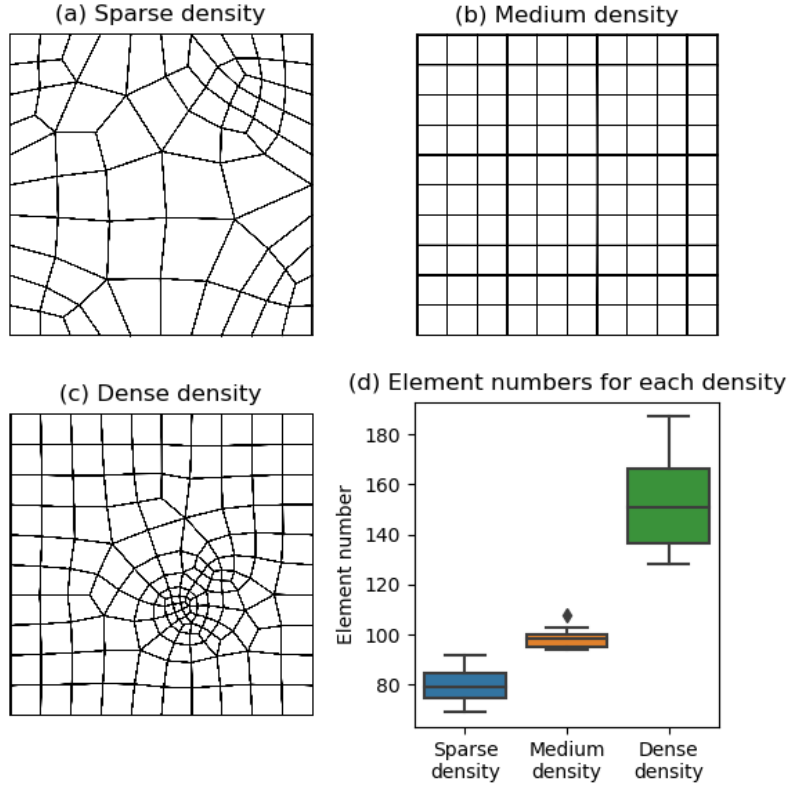


Figure 12: Different mesh densities controlled by the reward function. Three kinds of densities from sparse to dense, (a)-(c), are controlled by the parameter in the density term with  $v = 1.5, v = 1$ , and  $v = 0.5$ , respectively. Subfigure (d) shows the results of the number of generated elements by three kinds of densities averaged over 10 episodes, respectively.



solve training data problems by self-learning from the meshing process based on an RL algorithm, A2C. The introduced A2C method is only designed to provide training samples rather than offer an independent meshing model. The state representation and reward function are not well devised to allow the A2C to obtain the final meshing policy. It still needs to extract samples and train an FNN model, which hinders the automation to some extent.

FreeMesh-RL aims to learn the meshing policy in a fully automatic manner by redesigning the state representation and reward function, and exploiting the significant RL algorithm, SAC. With the guidance of the reward function, the agent can explore all the appropriate element positions for various boundary situations without human intervention. A fully automatic mesh generation method can be achieved, which is typically needed in current engineering communities.

Table 2: Comparison of learning methods used by various NN-based mesh generators. Four kinds of mesh generators that directly produce mesh elements using NN-based techniques are selected. The comparison focuses on mesh type, RL formulation, data source and algorithm of supervised learning.

Methods	Mesh type	Reinforcement learning			Supervised learning	
		State	Reward	Algorithm	Data	Algorithm
Papagiannopoulos et al. (2021)	Triangle	—	—	—	Gmsh	FNN
Yao et al. (2005)	Quadrilateral	—	—	—	Handcraft	FNN
Pan et al. (2021)	Quadrilateral	Neighboring points	$\sqrt{\eta_t^e * \eta_t^b}$	A2C	A2C	FNN
FreeMesh-RL	Quadrilateral	Neighboring points, area ratio	$\eta_t^e + \eta_t^b + \mu_t$	SAC	—	—

#### 4.2.2. Scalability verification

To validate the scalability of the learned meshing policy, we have constructed three geometry domains with the same shape but different vertex densities (i.e., 6.8 : 9.9 : 20.1, as shown in Table 4) on the boundaries. Three domains are meshed by the same trained RL model, and the results are shown in Table 3. It can be seen that all the domains have been successfully meshed; the elements on the boundaries are denser than in the interior area, which is beneficial for reducing computational burden; the transitions between dense and coarse meshes are smooth. We have also examined the meshing speed over three domains, which achieves 237 elements per second on average. Consequently, the results show that the self-learned mesh policy achieves good scalability to different scales of the meshing problem and is not constrained to the scale of the training domain. Many existing NN-based meshing methods, must train different models for adapting various sizes of domains, which is not practical for large-scale problems. The reason for this

adaptability is that the training domain will be continuously updated and evolved into various shapes that capture most boundary patterns (Pan et al., 2021).

Table 3: Meshing the same domain with different boundary segment densities by FreeMesh-RL. The boundary shapes of Domain 1-3 are the same, but the number of vertices on the boundary are from low to high. The scalability is examined through meshing all the domains with the same trained model.

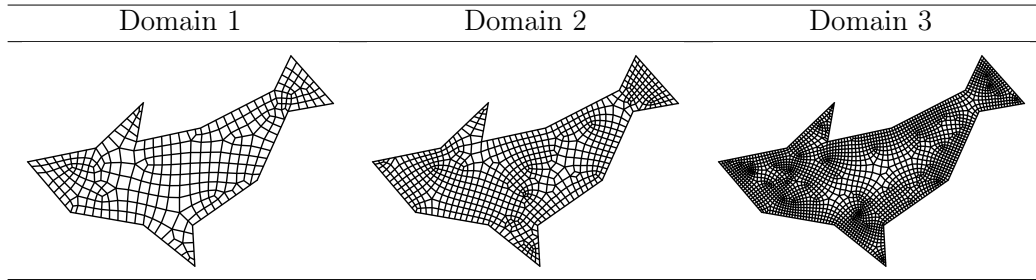


Table 4: Geometrical details of three domain boundaries and their generated meshes. The perimeter, the number of vertices and vertices per unit length on the initial boundaries of three domains are compared as well as their number of generated elements and meshing time.

	Domain 1	Domain 2	Domain 3
#vertices	102	150	304
Perimeter	15.1	15.1	15.1
#vertices per unit length	6.8	9.9	20.1
#elements	289	665	2157
Execution time (s)	0.9	2.6	15.3

#vertices - the number of vertices on the boundary.

#elements - the number of generated elements.

#### 4.2.3. Generalizability verification

To verify the generalizability of the obtained meshing model, we have meshed four different domains, Domains 4-7, using the obtained model. The shapes of the domains are from simple to complex. The meshing process and results are shown in Fig. 13. The general meshing process starts from

the boundary and advances inwardly to the central area of the domain. No matter the complexity of the initial domains, the boundary will evolve into different intermediate shapes according to the meshing policy. Obviously, the number of intermediate boundaries is equal to how many elements are generated. The execution number of the meshing policy over 4 domains is shown in Fig. 14. The meshing policy mainly consists of two types of rules (see type 0 and type 1 in Fig. 4), and the execution number of type 1 is around 80% of the total number. In Domain 7, there are 1489 intermediate boundaries in total; it can be said that the meshing policy succeeds in meshing 1489 different domain boundaries.

It can be noted that all the intermediate boundaries of 4 domains gradually become an oval shape. This demonstrates that the meshing policy can well solve hard boundary situations, such as sharp angles, and create smooth and easy situations for future element generation. It appears an evidence to show the effectiveness of the reward function design that considered the trade-off between the qualities of the current element and the remaining boundary.

Although the geometry shape can be diverse and infinite in real engineering applications, the proposed method only takes states of the boundary (i.e., partial boundaries) as the input, which guarantees that it is general to all the boundary shapes. As demonstrated above, the obtained policy is able to mesh hard situations while maintaining high quality of remaining boundaries. Therefore, the most challenging part of the whole meshing process is to mesh the initial boundary situations of a given domain. However, it can be easily solved by providing training domains with sufficient difficulties (in Fig. 9(a-c)). To conclude, the proposed method can be applied to arbitrary domains and is general to various geometries.

#### *4.2.4. Comparison to conventional methods*

To evaluate the meshing performance, we compare the quality of meshes by FreeMesh-RL against two widely adopted meshing approaches over three predefined 2D domain boundaries (i.e., domains D7-9). These domains possess different features, including sharp angles, bottleneck regions, unevenly distributed edges, and holes, to increase the testing diversity. The two conventional meshing approaches are Blossom-Quad (Remacle et al., 2012) and Pave (Blacker and Stephenson, 1991; White and Kinney, 1997). Blossom-Quad is an indirect method, which generates quadrilateral elements by finding the perfect matching of a pair of triangles generated in advance. The

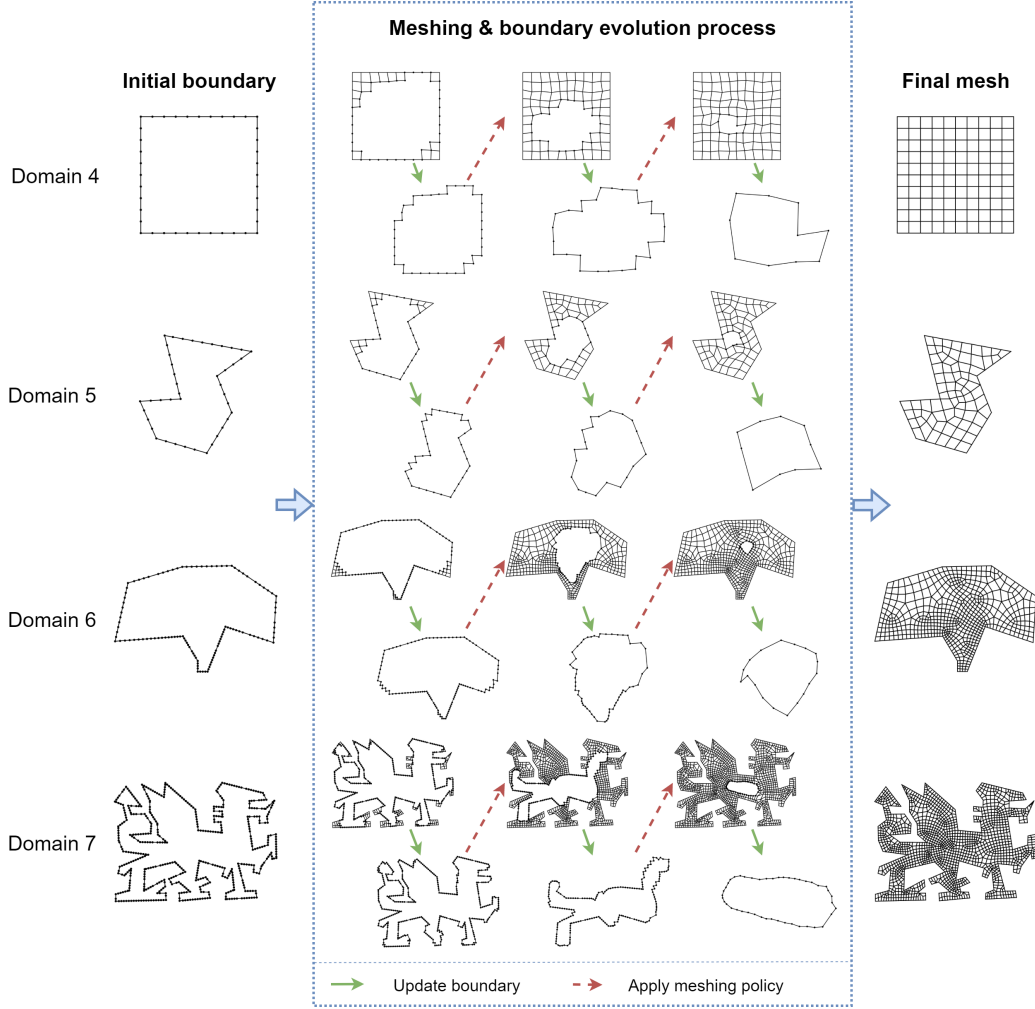


Figure 13: Model generalizability verification. Four different domains with shapes from simple to complex are selected; their meshing procedures are presented to exhibit the boundary evolution process and general meshing pattern by the learned policy. No matter how simple an initial shape was, the intermediate shapes can be complex; no matter how complex shape the initial boundary had, it gradually evolves into a smooth oval shape in the center of the domain.

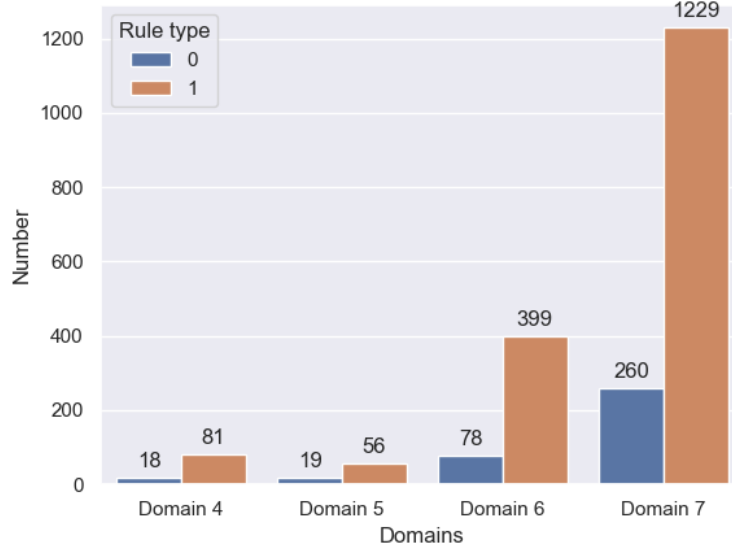


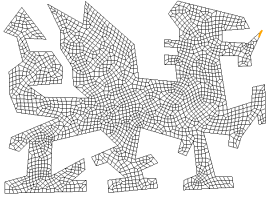
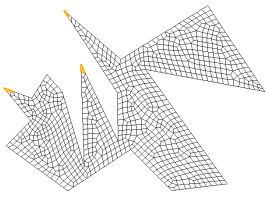
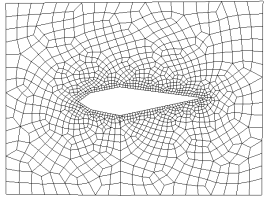
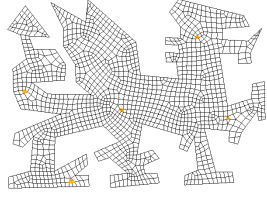
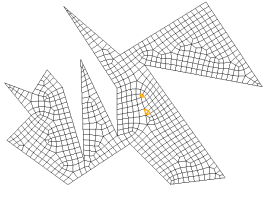
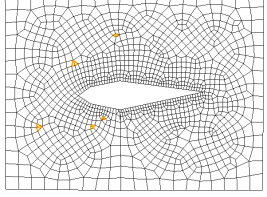
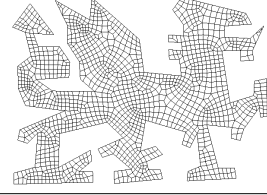
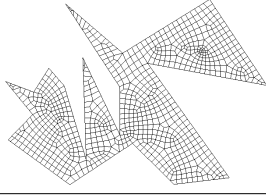
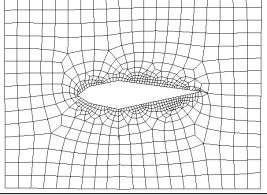
Figure 14: The evolution times of intermediate shapes are determined by how many times the meshing policy is executed. The execution numbers of the policy over the four domains are calculated, respectively. The meshing policy mainly consists of two types of rules: type 0 and 1. The number over each bar indicates the generating number of each rule type.

method is implemented by an open source generator Gmsh (Geuzaine and Remacle, 2009). Pave is another state-of-the-art meshing method for directly generating quadrilateral elements, which is implemented by the CUBIT software (Blacketer et al., 2016). Both of them are prevalent in the industry and haven’t been replaced by any machine learning-based methods yet, which are appropriate to be used as comparison methods.

The meshing results are shown in Table 5. Although all the methods can complete the meshes for the three domains, there are some subtle differences. Only FreeMesh-RL generates fully quadrilateral mesh. The other two methods have difficulties in discretizing the domains into full quadrilaterals and generate triangles in domains (marked in yellow colour in domains). Specifically, Blossom-Quad has a problem in handling domains with sharp angles on the boundary, while Pave has an issue in the interior of the domain. Extra operations (e.g., clean-ups) are usually required for these methods to eliminate triangles or bad quality elements, which slows down the meshing speed and decreases the automation to some extent. Contrarily, FreeMesh-RL doesn’t need those operations and avoids explicit treatments. Another advantage of FreeMesh-RL is that the generated mesh can easily grade from very small to large elements over a short distance, as shown in Table 5 Domain 9, which is beneficial for reducing computational burden during simulations (Shewchuk, 2012).

To quantitatively analyze the meshing results of three methods, we have selected eight common quality metrics to measure the meshing performance, including singularity (i.e., the number of irregular nodes whose number of incident edges in the interior of a mesh are not equal to four), element quality ( $\eta^e$  in Equation 6),  $|MinAngle - 90|$ ,  $|MaxAngle - 90|$ , scaled Jacobian, stretch, taper, and the number of triangles ( $\#triangles$ ) (Pan et al., 2021; Knupp et al., 2006). The measurement results are averaged over three domains and are shown in Table 6 and Fig. 15. FreeMesh-RL has achieved the best performance in the indices of singularity, taper, scaled Jacobian, and triangle. The smaller singularity means better regularity, which can provide better accurate results for numerical simulations. The smaller taper and bigger Scaled Jacobian represent the mesh element has a more regular shape like a square. If triangles exist, it indicates that the method is not full quadrilaterals and involves extra treatments to deal with them. The Pave method achieves the best performance in the other indices (i.e., element quality, min and max angles, and stretch). Blossom-Quad has the worse performance and is only slightly better than Pave as having fewer triangles. It is common for

Table 5: Meshing results comparison. Three types of domains are designed to examine the meshing performance based on the four identified criteria: a. sharp angle, b. narrow region, c. unevenly distributed boundary segments, and d. having a hole inside. Both Domain 7 and 8 possess features a and b, whereas Domain 9 has features c and d. Two representative methods, Blossom-Quad and Pave, are chosen to compare the meshing performance with the proposed method, FreeMesh-RL.

Algorithms	Domain 7	Domain 8	Domain 9
Blossom-Quad			
Pave			
FreeMesh-RL			

The elements in yellow represent existing triangles in the meshes.

indirect methods (i.e., Blossom-Quad) to have a suboptimal performance because they heavily rely on triangulation in advance. Remacle *et al.* Remacle et al. (2013) tried to optimize the triangulation. But the improvement is limited (Pan et al., 2021). The computational complexities for the three methods are also compared, which is all  $O(n^2)$ .

We also analyze the knowledge dependence on the algorithm development, as shown in Table 7. The development of meshing method can be briefly divided into three stages: pre-processing, element generation, and post-processing. Since the Blossom-Quad is an indirect quadrilateral mesh generation method, it requires the pre-processing of triangulation, which is unnecessary for the other two methods. To generate elements, the development of Blossom-Quad needs more complex geometry knowledge than Pave and FreeMesh-RL (see details in (Pan et al., 2021)). Pave, however, relies on lots of heuristic knowledge, which is time-consuming and inefficient for designers. FreeMesh-RL is the simplest method and only demands basic

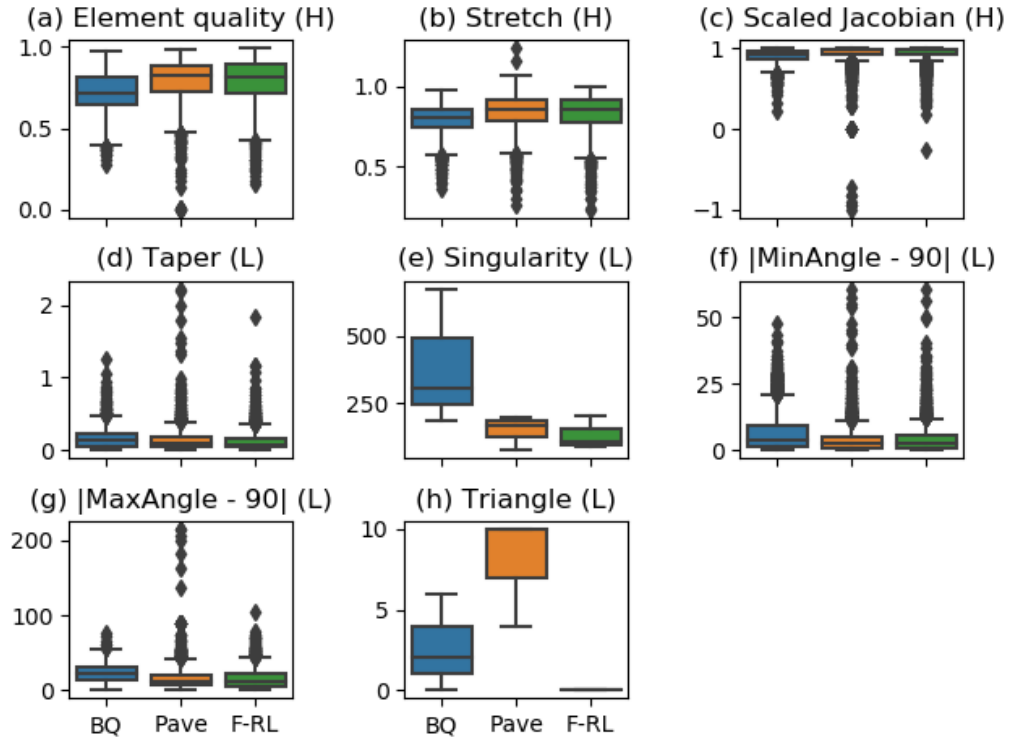


Figure 15: Meshing performance comparison results over eight kinds of quality indices. BQ represents the Blossom-Quad method; F-RL represents the FreeMesh-RL method. L, H indicate if the lower value or higher value is preferred, respectively.



Table 6: Quantitative measurement of the meshing performance of the three methods. All the quality metrics are averaged over the three domains.

Metrics	Blossom-Quad	Pave	FreeMesh-RL
Singularity (L)	$388 \pm 209.50$	$146.70 \pm 51.50$	<b><math>132 \pm 50</math></b>
Element quality (H)	$0.72 \pm 0.12$	<b><math>0.79 \pm 0.12</math></b>	$0.79 \pm 0.13$
$ MinAngle - 90 $ (L)	$6.55 \pm 6.91$	<b><math>3.69 \pm 4.60</math></b>	$4.02 \pm 5.10$
$ MaxAngle - 90 $ (L)	$22.16 \pm 11.14$	<b><math>15.69 \pm 14.71</math></b>	$15.73 \pm 12.48$
Scaled jacobian (H)	$0.91 \pm 0.08$	$0.94 \pm 0.13$	<b><math>0.94 \pm 0.10</math></b>
Stretch (H)	$0.79 \pm 0.08$	<b><math>0.84 \pm 0.10</math></b>	$0.83 \pm 0.11$
Taper (L)	$0.15 \pm 0.11$	$0.12 \pm 0.14$	<b><math>0.11 \pm 0.11</math></b>
Triangle (L)	$2.70 \pm 2.50$	$8 \pm 2.80$	<b><math>0 \pm 0</math></b>

L, H indicate if the lower value or higher value is preferred, respectively. The value in bold means the best among other approaches in that specific metric.

geometry concepts. As illustrated in the above meshing results, extra treatments as clean-ups are necessary for Blossom-Quad and Pave methods to remove triangles and bad elements while FreeMesh-RL is clean-up free.

Table 7: The comparison of knowledge dependence of three methods during the algorithm development. The algorithm development procedure is divided into three stages: pre-processing, element generation, and post-processing.

Steps	Blossom-Quad	Pave	FreeMesh-RL
Pre-processing	Delaunay triangulation	—	—
Element generation	Complex geometry knowledge	Heuristic knowledge	Basic geometry concepts
Post-processing	Clean-ups	Clean-ups	—

To conclude, the proposed method, FreeMesh-RL, is a highly cost-effective method that can fully automatically learn the meshing policy while performing in comparable quality to commercial systems. The learned policy can be applied to various domain boundaries without additional training and adjustment, which shows good generalizability and effectiveness.

## 5. Discussion

The proposed computational framework, FreeMesh-RL, has achieved several important improvements to both mesh generation and RL communities.

First, compared with conventional or NN-based mesh generation methods, FreeMesh-RL does not require heuristic knowledge or any labelled data, by using RL methods, particularly the SAC algorithm. It relieves people from

in-efficient searching for domain specific knowledge and time-consuming trial-and-error, and reduces the algorithm complexity by eliminating extra clean-up operations. Those obstacles greatly hinder the advancement of meshing methods towards high processing speed and mesh quality in complex geometry domains (Slotnick et al., 2014; Rushdi et al., 2017; Papagiannopoulos et al., 2021). Especially, for the 3D mesh generation problem, there is no automatic meshing solution yet because of the computational complexity and the difficulty in searching more complex heuristic knowledge. FreeMesh-RL proposes the easiest formulation of the meshing problem and can be applied to the 3D problem by virtue of the advancement of high performance computing and the self-learning properties of RL methods.

Second, the meshing policy in FreeMesh-RL can be self-learned by a well-defined reward function. The reward function determines various characteristics of the mesh, including mesh quality and density. Many downstream applications in FEA/CFD, usually require different mesh properties. In FreeMesh-RL, some of those requirements can be fulfilled by generating a customized mesh generator directly via adjusting the reward function rather than using extra expensive and time-consuming treatments, such as mesh adaption or remeshing. For instance, as shown in Fig. 12, the mesh density is controlled by a density factor in the reward function. Usually, more elements can provide accurate simulation results for applications but cost more computationally. In the graphic rendering area, the sparse mesh is preferred because of this reason. To adjust the mesh density is barely not applicable in any conventional mesh methods. This computational platform provides the easiest and cheapest fashion to design customized mesh generators.

Many RL topics are still not well understood (Duan et al., 2016). For instance, the designs of state representation and reward function are critical topics for the performance of RL algorithms and for understanding the mechanism of RL. The state representation will influence the generalizability, effectiveness, and learning speed (Niv, 2019; Lesort et al., 2018). To obtain the generalizability of the policy, a partial observation of the environment is hence utilized in FreeMesh-RL to eliminate the agent’s dependency on the global environment, which is the critical technique to achieve adaptability to other geometry domain environments. Many RL applications have to train different models for different environmental settings, which is not practical and expensive in real-life environments. As shown in the Fig. 11, how far the observation and how much information (i.e., vertices on the domain boundary) should be included are controlled by three factors, respectively.

The learning efficiency and overall return vary correspondingly. The low dimension state representation achieves better learning efficiency and provides easier interpretation and utilization for humans, thus improving the policy’s performance and generalizability. Some advanced topics for state representation may be researched in-depth by using this platform, such as partial observability, informative representations, state abstraction, and state representation learning (Dulac-Arnold et al., 2019; Lesort et al., 2018).

Finally, FreeMesh-RL has the potential to serve as an RL research platform, for example, to be used to study the reward function and examine the performance of RL algorithms. Many RL benchmark problems have very simple reward functions and environments, such as Atari games (Mnih et al., 2013), while some other famous problems are too complex, such as Dota2 (Berner et al., 2019) and StarCraft (Vinyals et al., 2017). The simple problems cannot fully reflect the performance of RL algorithms, whereas the complex problems cannot be easily used to study topics, such as hyperparameters tuning, generalizability, sample efficiency, and reward specification (Li, 2018). Mesh generation can be an excellent case to research RL. The difficulty of the mesh generation problem can be easily adjusted by altering the size and shape of input geometry domains. For example, as shown in 9, the SAC’s learning efficiency varies with the change of training domains, which offers a practical manner to interpret the internal mechanism of RL. The reward function can also be customized to fulfill different objectives, which is not applicable in many benchmark problems. As stated by Silver *et al.* (Silver et al., 2021), reward function is associated with almost all the agent’s behaviours that it can learn. With mesh generation, FreeMesh-RL can be developed as a testbed for understanding those topics.

There are a few limitations to the proposed method. FreeMesh-RL is limited to single connected 2D domains. To mesh multiply connected domains, one can manually turn them into a single connected domain and then use the trained policy (see (Pan et al., 2021)). The second limitation is that the meshing speed is not comparable with other conventional methods because it generates mesh element-by-element. A parallelization version could be the future work to solve this issue.

## 6. Conclusion

To overcome the difficulties of conventional methods in achieving the balance between high quality mesh and computational complexity, a novel

RL-based method for automatic quadrilateral mesh generation, FreeMesh-RL, is presented in this article. Since the geometry domains are naturally different and complex, a partial observation of the environment is adopted as the state to eliminate the agent’s dependency on the global environment and thus achieve adaptability to arbitrary meshing environments. The well designed reward function integrates the element quality, remaining boundary quality, and mesh density together, which allows the achievement of overall high mesh quality and the completeness of the meshing. Using extensive experiments on the various geometry domains, it was demonstrated that the proposed method could be adaptable to different environments and achieve competitive performance compared with representative commercial meshing software, while no complex post-processing operations are further needed. Consequently, FreeMesh-RL is a computationally efficient meshing framework that is fully automatic, can adapt to various complex geometries, and satisfies mesh quality requirements without extra treatments, which offers a feasible AI-based solution to general mesh generation problems.

Furthermore, this paper has discussed the potential of the FreeMesh-RL to be a computational platform to understand many RL topics, because of diverse meshing environments that control the problem difficulties, flexible state representation by altering the observation, and no fixed representation of the meshing objective that provides freedom for exploring the reward specification. Several future works can be conducted, such as the comparative analysis of deep RL algorithms using the FreeMesh-RL as the testbed, and the extension of this framework to the 3D mesh generation problem that is still challenging and unsolved.

## Acknowledgment

The support of the NSERC Discovery Grant (RGPIN-2019-07048) is gratefully acknowledged.

## References

Andrychowicz, M., Wolski, F., Ray, A., Schneider, J., Fong, R., Welinder, P., McGrew, B., Tobin, J., Abbeel, P., Zaremba, W., 2017. Hindsight experience replay. *arXiv:1707.01495* .

- Atalay, F.B., Ramaswami, S., Xu, D., 2008. Quadrilateral meshes with bounded minimum angle, in: Proceedings of the 17th International Meshing Roundtable. Springer, pp. 73–91.
- Baehmann, P.L., Wittchen, S.L., Shephard, M.S., Grice, K.R., Yerry, M.A., 1987. Robust, geometrically based, automatic two-dimensional mesh generation. *International Journal for Numerical Methods in Engineering* 24, 1043–1078.
- Bern, M., Eppstein, D., 2000. Quadrilateral meshing by circle packing. *International Journal of Computational Geometry & Applications* 10, 347–360.
- Berner, C., Brockman, G., Chan, B., Cheung, V., Dębiak, P., Dennison, C., Farhi, D., Fischer, Q., Hashme, S., Hesse, C., et al., 2019. Dota 2 with large scale deep reinforcement learning. *arXiv:1912.06680* .
- Blacker, T.D., Owen, S.J., Staten, M.L., Quadros, W.R., Hanks, B., Clark, B.W., Meyers, R.J., Ernst, C., Merkley, K., Morris, R., et al., 2016. CUBIT geometry and mesh generation toolkit 15.2 user documentation. Technical Report. Sandia National Lab.(SNL-NM), Albuquerque, NM (United States).
- Blacker, T.D., Stephenson, M.B., 1991. Paving: A new approach to automated quadrilateral mesh generation. *International journal for numerical methods in engineering* 32, 811–847.
- Bommes, D., Lévy, B., Pietroni, N., Puppo, E., Silva, C., Tarini, M., Zorin, D., 2013. Quad-mesh generation and processing: A survey 32, 51–76.
- Brewer, M.L., Diachin, L.F., Knupp, P.M., Leurent, T., Melander, D.J., 2003. The mesquite mesh quality improvement toolkit., in: IMR.
- Chen, R.T., Rubanova, Y., Bettencourt, J., Duvenaud, D., 2018. Neural ordinary differential equations. *arXiv:1806.07366* .
- Cheng, G., Li, H., 1996. New method for graded mesh generation of quadrilateral finite elements. *Computers & structures* 59, 823–829.
- Chew, L.P., 1989. Constrained delaunay triangulations. *Algorithmica* 4, 97–108.

- Daniels, J., Silva, C.T., Shepherd, J., Cohen, E., 2008. Quadrilateral mesh simplification. *ACM transactions on graphics (TOG)* 27, 1–9.
- Defferrard, M., Bresson, X., Vandergheynst, P., 2016. Convolutional neural networks on graphs with fast localized spectral filtering. *Advances in neural information processing systems* 29, 3844–3852.
- Docampo-Sanchez, J., Haimes, R., 2019. Towards fully regular quad mesh generation, in: *AIAA Scitech 2019 Forum*, p. 1988.
- Duan, Y., Chen, X., Houthoofd, R., Schulman, J., Abbeel, P., 2016. Benchmarking deep reinforcement learning for continuous control, in: *International conference on machine learning*, PMLR. pp. 1329–1338.
- Dulac-Arnold, G., Mankowitz, D., Hester, T., 2019. Challenges of real-world reinforcement learning. *arXiv:1904.12901* .
- Fujimoto, S., Hoof, H., Meger, D., 2018. Addressing function approximation error in actor-critic methods, in: *International Conference on Machine Learning*, PMLR. pp. 1587–1596.
- Garimella, R.V., Shashkov, M.J., Knupp, P.M., 2004. Triangular and quadrilateral surface mesh quality optimization using local parametrization. *Computer Methods in Applied Mechanics and Engineering* 193, 913–928.
- Geuzaine, C., Remacle, J.F., 2009. Gmsh: A 3-d finite element mesh generator with built-in pre-and post-processing facilities. *International journal for numerical methods in engineering* 79, 1309–1331.
- Gordon, W.J., Hall, C.A., 1973. Construction of curvilinear co-ordinate systems and applications to mesh generation. *International Journal for Numerical Methods in Engineering* 7, 461–477.
- Gottesman, O., Johansson, F., Komorowski, M., Faisal, A., Sontag, D., Doshi-Velez, F., Celi, L.A., 2019. Guidelines for reinforcement learning in healthcare. *Nature medicine* 25, 16–18.
- Gupta, K., 2020. Neural Mesh Flow: 3D Manifold Mesh Generation via Diffeomorphic Flows. University of California, San Diego.

- Haarnoja, T., Zhou, A., Abbeel, P., Levine, S., 2018a. Soft actor-critic: Off-policy maximum entropy deep reinforcement learning with a stochastic actor, in: International Conference on Machine Learning, PMLR. pp. 1861–1870.
- Haarnoja, T., Zhou, A., Hartikainen, K., Tucker, G., Ha, S., Tan, J., Kumar, V., Zhu, H., Gupta, A., Abbeel, P., et al., 2018b. Soft actor-critic algorithms and applications. arXiv:1812.05905 .
- Hanocka, R., Hertz, A., Fish, N., Giryes, R., Fleishman, S., Cohen-Or, D., 2019. Meshcnn: a network with an edge. ACM Transactions on Graphics (TOG) 38, 1–12.
- Kaelbling, L.P., Littman, M.L., Moore, A.W., 1996. Reinforcement learning: a survey. Journal of artificial intelligence research 4, 237–285.
- Knupp, P.M., Ernst, C., Thompson, D.C., Stimpson, C., Pebay, P.P., 2006. The verdict geometric quality library. Technical Report. Sandia National Laboratories.
- Lesort, T., Díaz-Rodríguez, N., Goudou, J.F., Filliat, D., 2018. State representation learning for control: An overview. Neural Networks 108, 379–392.
- Li, Y., 2018. Deep reinforcement learning. arXiv:1810.06339 .
- Liang, X., Ebeida, M.S., Zhang, Y., 2010. Guaranteed-quality all-quadrilateral mesh generation with feature preservation. Computer Methods in Applied Mechanics and Engineering 199, 2072–2083.
- Liang, X., Zhang, Y., 2012. Matching interior and exterior all-quadrilateral meshes with guaranteed angle bounds. Engineering with Computers 28, 375–389.
- Lillicrap, T.P., Hunt, J.J., Pritzel, A., Heess, N., Erez, T., Tassa, Y., Silver, D., Wierstra, D., 2015. Continuous control with deep reinforcement learning. arXiv:1509.02971 .
- Liu, C., Yu, W., Chen, Z., Li, X., 2017. Distributed poly-square mapping for large-scale semi-structured quad mesh generation. Computer-Aided Design 90, 5–17.

- Machado, M.C., Bellemare, M.G., Talvitie, E., Veness, J., Hausknecht, M., Bowling, M., 2018. Revisiting the arcade learning environment: Evaluation protocols and open problems for general agents. *Journal of Artificial Intelligence Research* 61, 523–562.
- Mazyavkina, N., Sviridov, S., Ivanov, S., Burnaev, E., 2021. Reinforcement learning for combinatorial optimization: A survey. *Computers & Operations Research* , 105400.
- Mnih, V., Badia, A.P., Mirza, M., Graves, A., Lillicrap, T., Harley, T., Silver, D., Kavukcuoglu, K., 2016. Asynchronous methods for deep reinforcement learning, in: *International conference on machine learning*, PMLR. pp. 1928–1937.
- Mnih, V., Kavukcuoglu, K., Silver, D., Graves, A., Antonoglou, I., Wierstra, D., Riedmiller, M., 2013. Playing atari with deep reinforcement learning. *arXiv:1312.5602* .
- Nechaeva, O., 2006. Composite algorithm for adaptive mesh construction based on self-organizing maps, in: *International Conference on Artificial Neural Networks*, Springer. pp. 445–454.
- Niv, Y., 2019. Learning task-state representations. *Nature neuroscience* 22, 1544–1553.
- Osband, I., Doron, Y., Hessel, M., Aslanides, J., Sezener, E., Saraiva, A., McKinney, K., Lattimore, T., Szepesvari, C., Singh, S., et al., 2019. Behaviour suite for reinforcement learning. *arXiv:1908.03568* .
- Owen, S.J., 1998. A survey of unstructured mesh generation technology, in: *IMR*, p. 267.
- Pan, J., Huang, J., Wang, Y., Cheng, G., Zeng, Y., 2021. A self-learning finite element extraction system based on reinforcement learning. *Artificial Intelligence for Engineering Design, Analysis and Manufacturing* 35, 180–208. doi:10.1017/S089006042100007X.
- Papagiannopoulos, A., Clausen, P., Avellan, F., 2021. How to teach neural networks to mesh: Application on 2-d simplicial contours. *Neural Networks* 136, 152–179.



- Raffin, A., Hill, A., Gleave, A., Kanervisto, A., Ernestus, M., Dormann, N., 2021. Stable-baselines3: Reliable reinforcement learning implementations. *Journal of Machine Learning Research* .
- Remacle, J.F., Henrotte, F., Carrier-Baudouin, T., Béchet, E., Marchandise, E., Geuzaine, C., Mouton, T., 2013. A frontal delaunay quad mesh generator using the  $l_\infty$  norm. *International Journal for Numerical Methods in Engineering* 94, 494–512.
- Remacle, J.F., Lambrechts, J., Seny, B., Marchandise, E., Johnen, A., Geuzainet, C., 2012. Blossom-quad: A non-uniform quadrilateral mesh generator using a minimum-cost perfect-matching algorithm. *International journal for numerical methods in engineering* 89, 1102–1119.
- Roca, X., Loseille, A., 2019. 27th International Meshing Roundtable. volume 127. Springer.
- Rushdi, A.A., Mitchell, S.A., Mahmoud, A.H., Bajaj, C.C., Ebeida, M.S., 2017. All-quad meshing without cleanup. *Computer-Aided Design* 85, 83–98.
- Schulman, J., Wolski, F., Dhariwal, P., Radford, A., Klimov, O., 2017. Proximal policy optimization algorithms. *arXiv:1707.06347* .
- Shewchuk, J.R., 2012. Unstructured mesh generation. *Combinatorial Scientific Computing* 12, 2.
- Shimada, K., Liao, J.H., Itoh, T., 1998. Quadrilateral meshing with directionality control through the packing of square cells, in: *IMR, Citeseer*. pp. 61–75.
- Silver, D., Huang, A., Maddison, C.J., Guez, A., Sifre, L., Van Den Driessche, G., Schrittwieser, J., Antonoglou, I., Panneershelvam, V., Lanctot, M., et al., 2016. Mastering the game of go with deep neural networks and tree search. *Nature* 529, 484–489.
- Silver, D., Singh, S., Precup, D., Sutton, R.S., 2021. Reward is enough. *Artificial Intelligence* , 103535.
- Slotnick, J., Khodadoust, A., Alonso, J., Darmofal, D., Gropp, W., Lurie, E., Mavriplis, D., 2014. Cfd vision 2030 study: a path to revolutionary computational aerosciences.

- Sutton, R.S., Barto, A.G., 2018. Reinforcement learning: an introduction. MIT press.
- Verma, C.S., Suresh, K., 2017. A robust combinatorial approach to reduce singularities in quadrilateral meshes. *Computer-Aided Design* 85, 99–110.
- Verma, C.S., Suresh, K., 2018.  $\alpha$ mst: A robust unified algorithm for quadrilateral mesh adaptation in 2d and 3d. *Computer-Aided Design* 103, 47–60.
- Vinyals, O., Ewalds, T., Bartunov, S., Georgiev, P., Vezhnevets, A.S., Yeo, M., Makhzani, A., Küttler, H., Agapiou, J., Schrittwieser, J., et al., 2017. Starcraft ii: A new challenge for reinforcement learning. *arXiv:1708.04782*.
- Vinyals, O., Fortunato, M., Jaitly, N., 2015. Pointer networks, in: *Advances in Neural Information Processing Systems*, Curran Associates, Inc.
- Wang, N., Zhang, Y., Li, Z., Fu, Y., Liu, W., Jiang, Y.G., 2018a. Pixel2mesh: Generating 3d mesh models from single rgb images, in: *Proceedings of the European Conference on Computer Vision (ECCV)*, pp. 52–67.
- Wang, W.Y., Li, J., He, X., 2018b. Deep reinforcement learning for nlp, in: *Proceedings of the 56th Annual Meeting of the Association for Computational Linguistics: Tutorial Abstracts*, pp. 19–21.
- Wang, Z., Schaul, T., Hessel, M., Hasselt, H., Lanctot, M., Freitas, N., 2016. Dueling network architectures for deep reinforcement learning, in: *International conference on machine learning*, PMLR. pp. 1995–2003.
- Wei, Q., Wang, L., Liu, Y., Polycarpou, M.M., 2020. Optimal elevator group control via deep asynchronous actor–critic learning. *IEEE transactions on neural networks and learning systems* 31, 5245–5256.
- Wen, C., Zhang, Y., Li, Z., Fu, Y., 2019. Pixel2mesh++: Multi-view 3d mesh generation via deformation, in: *Proceedings of the IEEE/CVF International Conference on Computer Vision*, pp. 1042–1051.
- White, D.R., Kinney, P., 1997. Redesign of the paving algorithm: Robustness enhancements through element by element meshing, in: *6th International Meshing Roundtable*, Citeseer. p. 830.

- Yang, J., Dzanic, T., Petersen, B., Kudo, J., Mittal, K., Tomov, V., Camier, J.S., Zhao, T., Zha, H., Kolev, T., et al., 2021. Reinforcement learning for adaptive mesh refinement. *arXiv:2103.01342* .
- Yao, S., Yan, B., Chen, B., Zeng, Y., 2005. An ann-based element extraction method for automatic mesh generation. *Expert Systems with Applications* 29, 193–206.
- Zeng, Y., Cheng, G., 1991. On the logic of design. *Design Studies* 12, 137–141.
- Zeng, Y., Cheng, G., 1993. Knowledge-based free mesh generation of quadrilateral elements in two-dimensional domains. *Computer-Aided Civil and Infrastructure Engineering* 8, 259–270.
- Zeng, Y., Yao, S., 2009. Understanding design activities through computer simulation. *Advanced Engineering Informatics* 23, 294–308.
- Zhang, Z., Wang, Y., Jimack, P.K., Wang, H., 2020. Meshingnet: A new mesh generation method based on deep learning, in: *International Conference on Computational Science*, Springer. pp. 186–198.
- Zhu, J., Zienkiewicz, O., Hinton, E., Wu, J., 1991. A new approach to the development of automatic quadrilateral mesh generation. *International Journal for Numerical Methods in Engineering* 32, 849–866.
- Ziebart, B.D., 2010. Modeling purposeful adaptive behavior with the principle of maximum causal entropy. Carnegie Mellon University.